Enhanced impurity-induced damping of magnetic modes in FeF$_2$:Mn

R. M. Toussaint, D. W. Hone, and V. Jaccarino

Department of Physics, University of California, Santa Barbara, California 93106

S. M. Rezende

Department of Physics, University of California, Santa Barbara, California 93106
and Departamento de Física, Universidade Federal de Pernambuco, 50000 Recife, Pernambuco, Brazil

High-resolution far-infrared laser spectroscopy is used to investigate the impurity-induced relaxation of the $k \simeq 0$ host mode in antiferromagnetic FeF$_2$:Mn at low temperatures, for Mn-impurity concentrations $c \simeq (2-5) \times 10^{-3}$ at. %. The transmission spectra exhibit very asymmetric broadening with increasing c, with the modes above the polariton gap having linewidths nearly an order of magnitude larger than the antiferromagnetic resonance. The observed frequency-dependent relaxation (formally, a frequency-dependent imaginary self-energy) is shown to arise from two magnon impurity scattering. However, the close proximity of the impurity mode to the host magnon band requires the inclusion of multiple-scattering effects to obtain quantitative agreement between experiment and theory.

I. INTRODUCTION

Since both the exchange and anisotropy fields are large, the antiferromagnetic resonance (AFMR) frequency of FeF$_2$ lies in the far-infrared (FIR) region (1.575 THz, or 189 μm for zero applied magnetic field). Because of this, the early AFMR studies on FeF$_2$ utilized grating or Fourier-transform[1,2] FIR spectrometers, which lack the resolution of, for example, microwave magnetic resonance spectrometers. With the development of FIR lasers, high-resolution AFMR and local mode studies of FeF$_2$ and FeF$_2$:Mn were made which revealed many new facets of the $k \simeq 0$ spin excitations in this system.[3,4]

Contrary to conventional magnetic resonance experiments where the wavelength of the radiation is much larger than the sample dimension d, in the FIR experiments $\lambda \simeq d$. As a result, propagation effects of the exciting radiation are important. Instead of just probing the AFMR, the FIR field generates propagating coupled photon-magnon modes, or *magnetic polaritons*[5] in the sample. Previous studies of the magnetic polaritons in FeF$_2$ include the detailed analysis of the very broad and asymmetric line shape observed in transmission experiments[3,4] and the measurement of the polariton absorption[6] and group velocity versus wave vector $\vec{k}$.[7] One can account in detail for all of the observed properties in pure (or essentially pure) FeF$_2$ by inclusion of a frequency-independent damping in the equations of motion. When a Mn impurity is introduced into FeF$_2$ a local mode appears very close to the bottom of the host magnon band. For small concentrations of Mn ($c < 1$ at. %) the frequency pulling effects can be accurately obtained by treating the host and impurity sublattice magnetizations using two sets of coupled equations of motion. However, neither the broadening of the impurity nor that of the host modes is adequately described by introducing a frequency *independent* damping—particularly so as the concentration of Mn

increases beyond $c \sim 0.01$ at. %. The impurity mode damping has been studied in detail and the dominant relaxation mechanisms have been clearly identified.[4,8-10]

In this paper the problem of the broadening of the host modes by the Mn impurities is investigated. The most significant experimental fact is that the observed relaxation rate is strongly frequency dependent and its value above the polariton gap is more than two orders of magnitude larger than one would expect from lowest order two-magnon (exchange or anisotropy) scattering.[11] The reason for this is that the local perturbation potential associated with the Mn impurity is so strong that a bound state (local magnon) appears; hence, the usual perturbation theory (Fermi golden rule) result is not directly applicable. We show that inclusion of multiple-scattering effects to all orders, through introduction of the t matrix, corrects this problem and accounts for the measured linewidths.

In Sec. II the main features of magnetic polaritons in antiferromagnets are given. In Sec. III the experiments are described and the data are presented. Section IV is devoted to the calculation of the two-magnon scattering contribution to the linewidth. A discussion of the results appears in Sec. V.

II. MAGNETIC POLARITONS

The propagation in an antiferromagnet of the coupled magnon-photon excitations called "magnetic polaritons" can be simply determined within an effective-field, coupled equations of motion approach for the magnetization.[4] For a two-sublattice uniaxial antiferromagnet (AF), with an applied magnetic field $\vec{H}_0$ parallel to the unique axis (z direction) and driven by a spatially uniform rotating field of frequency ω, the frequency- and field-dependent transverse susceptibility is

$$\chi^{\pm}(\omega, H_0) = 2H_A M / \{ H_c^2 - [(\omega/\gamma) \mp H_0]^2 \} , \tag{1}$$

where γ is the gyromagnetic ratio, M is the sublattice magnetization, $H_c = (2H_E H_A + H_A^2)^{1/2}$, and H_A and H_E are the anisotropy and exchange fields, respectively. The propagation and volume dipolar effects are contained in Maxwell's equations. When these are solved with the appropriate permeability tensor obtained from (1) for plane waves propagating with $\vec{k}||\vec{H}_0$, the following polariton dispersion results:[4]

$$k^{\pm} = \frac{\omega \epsilon^{1/2}}{c} \left[1 + \frac{8\pi M H_A}{H_c^2 - [(\omega/\gamma) \mp H_0]^2} \right]^{1/2}, \quad (2)$$

where ϵ is the dielectric constant and c is the speed of light. This dispersion is shown in Fig. 1 for FeF_2 with $\vec{H}_0 = 0$ in the case of no damping (ω real). The poles of $k^{\pm}$ are the up- and down-going resonance frequencies in an infinite medium, $\omega_{\vec{H}}^{\pm} = \gamma (H_c \pm H_0)$. When ω is close to ω_H (1.57 THz in FeF_2 at $H_0 = 0$) the modes are hybrid magnon-photon excitations. Between ω_H and $\omega_H + \gamma \Delta_{FB}$, where $\Delta_{FB} \simeq 4\pi M H_A / H_c$ (2.8 kOe or 8.4 GHz in FeF_2), there is a "forbidden band" for propagation, within which $k^{\pm}$ has no real solution. In the region far off resonance, Eq. (2) approaches the photon dispersion relation $k = \omega \epsilon^{1/2}/c$. For waves propagating with $\vec{k} \perp \vec{H}_0$ a dispersion relation similar to (2) is obtained, but in this case the forbidden band extends from $\omega_1 \simeq \omega_H + \Delta_{FB}/2$ (the top of the spin-wave manifold at $k = 0$) to $\omega_H + \gamma \Delta_{FB}$.

The forbidden band of Fig. 1 has a drastic effect on the line shape of the transmitted radiation through a sample of finite thickness, from which important information about the magnetic properties can be obtained. The FIR radiation transmission line shapes resulting from the complex wave vectors in (2), with the inclusion of damping, were discussed in detail in Ref. 4. Those results will be used to extract the information on the magnetic damping from the data presented in Sec. III.

III. EXPERIMENTAL OBSERVATIONS

Direct transmission measurements at 4.2 K of the AFMR spectra were made with a far-infrared laser—
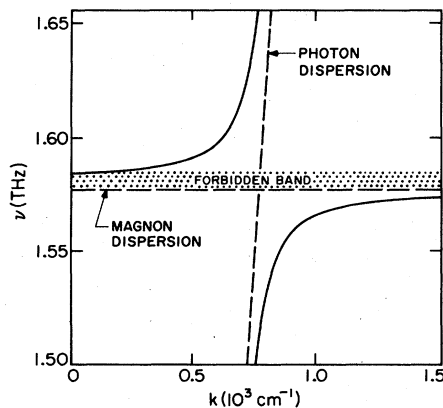
superconducting-solenoid spectrometer described elsewhere.[4] Spectra were obtained at a fixed frequency of $\nu = 1.3623$ THz (H_2O-vapor laser line) by sweeping the external magnetic field H_0 applied parallel to the unique ($\hat{c}$) axis of the crystal. The radiation ($\hat{k}||\hat{c}$) was incident normal to the faces (polished to within 1 μm) of disk-shaped samples, typically 4 mm in diameter and 100-μm-thick FeF_2 crystals with Mn impurity concentration $c = 0.0014$, 0.3, and 0.5 at. %, as determined from the relative intensities of the impurity-associated and host ^{19}F NMR spectra.

We first review what is observed in pure FeF_2 to understand the changes that occur in the line profile as the impurity concentration is increased. In Fig. 2 the transmission spectrum of a 77-μm-thick sample of nearly pure FeF_2 ($c = 0.0014$ at. %) is shown by the solid line. The dashed curve represents the theoretical prediction obtained using the analysis given in Ref. 4 with a Lorentzian linewidth of $\Delta H = 20$ Oe, which is introduced by letting $\omega \rightarrow \omega + i\Delta\omega$ in the equations of motion, with $\Delta\omega = \gamma \Delta H/2$. Several important features of the spectrum in Fig. 2, denoted by the letters $A - F$, can be qualitatively understood. Far off resonance (A,F) the wave vector $\vec{k}$ is entirely real and varies slowly with H_0. Therefore, the transmission, which depends on the thickness t and k, is almost constant. Approaching the resonance position, Re k varies rapidly and gives rise to the interference peaks which are labeled B and E. At the resonance position, Im k varies from zero to its maximum value, causing the steep slope in the spectrum labeled C. The sharp corner (low field) corresponds to the down-going AFMR position. The flat section of the transmission curve (D) is a consequence of the forbidden band, where k is entirely imaginary. The slope near the AFMR position, the width of the flat region, and the intensity of the interference peaks are all very sensitive to the value of the linewidth. In fact, comparison between computer-generated transmission spectra for various linewidths and the data can be used to determine ΔH with reasonable accuracy. The

FIG. 1. Calculated magnetic polariton dispersion in FeF_2 at $H_0 = 0$ for propagation along the symmetry direction.
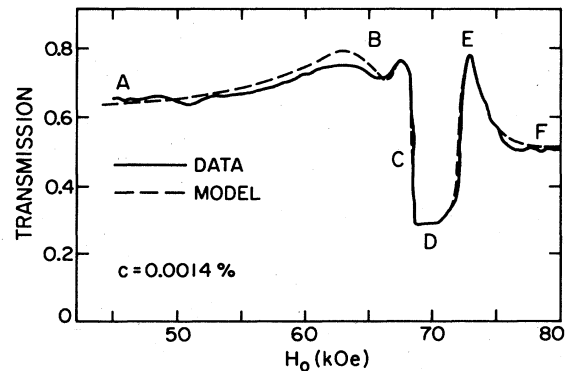

FIG. 2. Measured transmission spectrum of $\nu = 1.3623$ THz radiation through a 77-μm-thick sample of FeF_2 at $T = 4.2$ K (0.0014±0.0007 at. % Mn) shown by the solid line. The dashed line is the prediction of the polariton model with $H = 20$ Oe, Ref. 4.

small value of $\Delta H \simeq 20$ Oe measured in the nearly-pure FeF_2 sample was[4] attributed almost entirely to radiation broadening;[12] that is to say, as the impurity concentration goes to zero, the damping of the magnetic polariton results mainly from the photon admixture.

The observed spectrum changes markedly with the introduction of Mn even in small quantities such as $c > 0.2$ at. %. First, a strong impurity-associated local mode appears below and very close to the host mode.[4,8−10] The transmission spectra of the host mode for two different concentrations—$c = 0.3$ at. % ($t = 105$ μm) and $c = 0.5$ at. % ($t = 80$ μm)—are shown in Fig. 3. With increasing concentration, the mode shifts in frequency and the line profile broadens. A most important feature to be noted is that the low-field edge, corresponding to the AFMR frequency, remains relatively sharp. However, the high-field edge of the line, which corresponds to polaritons above the forbidden band, broadens rapidly with increasing c. This is seen most clearly in the lower half of the figure, where the 0.3 at. %—Mn spectrum (shown by the dashed curve) has been shifted so that the AFMR positions of the two spectra coincide. Although the model provided excellent fits to transmission spectra of 0.0014 at. % $Mn:FeF_2$ with $\Delta H = 20$ Oe, the higher concentration spectra cannot be fitted with *any* choice of a single Lorentzian linewidth. For example, Fig. 4 shows two attempts to fit the $c = 0.5$ at. % data (solid line) with a single frequency-independent linewidth. The value required to fit the AFMR edge (dashed-dotted line) is $\Delta H = 0.5$ kOe, which is an order of magnitude lower than $\Delta H = 5.0$ kOe needed to fit the line shape above the forbidden band. Similarly, for the $c = 0.3$ at. % sample we determine $\Delta H = 0.1$ and 1.0 kOe, respectively, for the AFMR and the top of the polariton bandwidths.

FIG. 4. Transmission line profile observed (solid line) for a 80-μm-thick sample of 0.5 at. % $Mn:FeF_2$ compared to results of calculation with two different frequency independent linewidths for the host mode. Clearly the ΔH required to fit the AFMR edge is substantially less than that needed to fit the top of the polariton band.

IV. THEORY

The two most significant features of the linewidth data of the preceding section can be summarized as follows: (1) The AFMR linewidth of FeF_2 with Mn impurities increases rapidly with the impurity concentration c, and (2) the polariton damping in the impure crystal is a strong function of its frequency relative to the AFMR position. One of the features of the data can be accounted for by a linewidth transfer mechanism.[4] The Mn impurity-associated local mode lies below and very close to the AFMR frequency. The linewidth ΔH_I of this mode is substantially larger than that of the host AFMR and it increases rapidly with c ($\Delta H_I = 6$ and 12.5 kOe for $c = 0.3$ and 0.5 at. %, respectively, at $\nu = 1.36$ THz) as a result of the impurity-impurity interaction.[8] If the measured ΔH_I is introduced phenomenologically in the impurity magnetization equation of motion, and no damping is used in the host equations, the broadening of the AFMR mode with increasing concentration is reasonably well predicted for $c > 0.01$ at. %. However, this mechanism cannot account for the much larger damping required to fit the line shape above the polariton forbidden band. As is shown below, the strongly frequency-dependent mechanism required to explain the data is the enhanced impurity two-magnon scattering.

It is well known that two-magnon scattering, in which a magnon of wave vector $\vec{k}$ decays via scattering by aperiodic defects into degenerate magnons with $\vec{k}' \neq \vec{k}$, provides the dominant broadening mechanism of $k = 0$ modes in ferromagnets and antiferromagnets at $T = 0$ K.[13] Comparison between experiment and theory in antiferromagnets has been confined to MnF_2, in which AFMR line width studies have been made in the microwave (9—24 GHz) region.[14−16] In this case, the surface demagnetizing energy shifts the $k \simeq 0$ mode into the degenerate manifold of spin-wave states, where it can decay into oth-
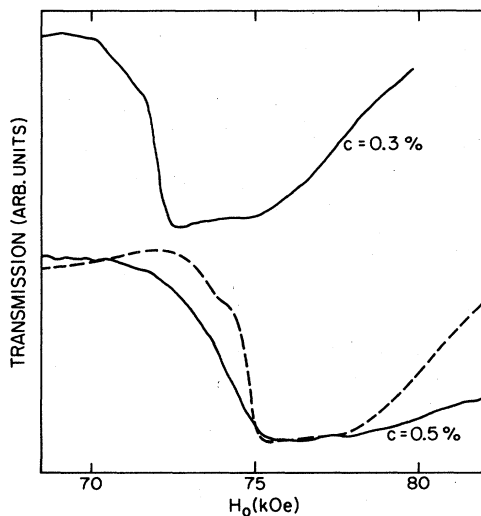

FIG. 3. Measured host-mode line profiles for two concentrations of Mn impurities at $\nu = 1.3623$ THz and 4.2 K. With increasing concentration, the mode shifts in frequency and broadens. The $c = 0.3$ at. % spectrum has been shifted (dashed curve) to facilitate comparison with the $c = 0.5$ at. % spectrum. Notice that the high-field side of the polariton line broadens more rapidly with increasing c.
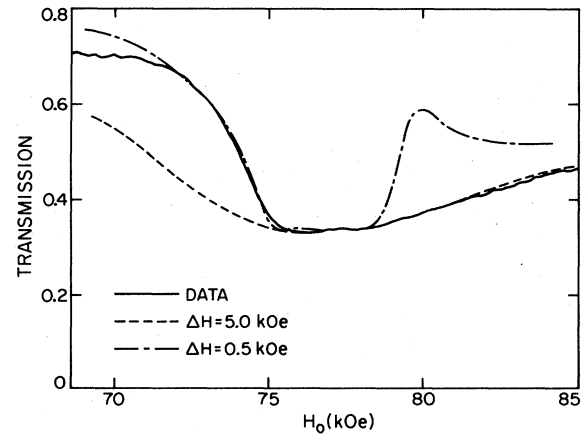
er magnons with $k \neq 0$. Linewidths of $0.05 < \Delta H < 20$ Oe ($T \ll T_N$) have been measured for the uniform and magnetostatic modes in highly-polished disks of MnF_2, and have been shown to be associated with two-magnon scattering and radiation damping.[12,14–16] However, for FeF_2 the studies must be conducted in the far infrared, and the excited modes have $kd \gg 1$, where d is a characteristic sample dimension. In this case the transverse component of the rf magnetization varies rapidly across the sample, averaging the surface demagnetizing fields to zero. Thus the AFMR energy is raised only a negligible amount relative to the bottom of the degenerate spin-wave band, where the density of degenerate states is very small. Hence the two-magnon scattering is not expected to be a significant source of broadening at the AFMR position. However, the magnetic admixture of the polaritons near the top of the forbidden band is degenerate with a much larger manifold of spin-wave states and thus can more readily decay via two-magnon scattering.

Clearly this mechanism exhibits the essential feature for a frequency-dependent damping. The conventional treatment developed by Loudon and Pincus[11] is perturbative in the defect potential. Although we recognize that an impurity scatterer which has associated with it a local mode (bound state) close to the bottom of the host magnon band cannot be so treated, we first develop the calculation in that way. We will then show that the modifications necessary to properly deal with multiple scattering effects involve only a straightforward replacement of bare potential by t-matrix elements.

Far from the polariton region ($k \gg 10^3$ cm^{-1} in FeF_2) the dispersion relation of the magnetic excitations can be calculated with Zeeman, exchange, anisotropy, and volume dipolar contributions. For H_0 parallel to the c axis, the AF dispersion relation for $ka \ll 1$, where a is the separation between spins on the same sublattice in the plane perpendicular to $\hat{c}$, is given by

$$\omega_k/\gamma \simeq (H_c^2 + 4\pi MH_A \sin^2\theta_k + 2H_E^2 b^2 k^2)^{1/2} \pm H_0 \quad (3)$$

where $b = a/z^{1/2}$, z is the number of next-nearest neighbors, and θ_k is the angle $\vec{k}$ makes with the c axis. Equation (3) is valid in the limit where $H_0(H_c + H_0) \gg 2\pi MH_A$ and $H_A \gg H_E b^2 k^2$. Since these results were applied to measurements on the lower branch of FeF_2 with $H_0 \simeq 90$ kOe, this limit is applicable. Equation (3) is plotted versus k in Fig. 5 and shows the degenerate manifold of spin-wave states which exist for $\omega_k > \gamma(H_c + H_0) \equiv \omega_H^+$. Modes in this frequency range can therefore scatter via two-magnon processes and conserve energy.

Since aperiodic defects destroy the translational invariance of the pure lattice they allow processes in which crystal momentum is not conserved. The Hamiltonian can be expressed in the form

$$\mathcal{H} = \mathcal{H}_0 + V, \quad (4)$$

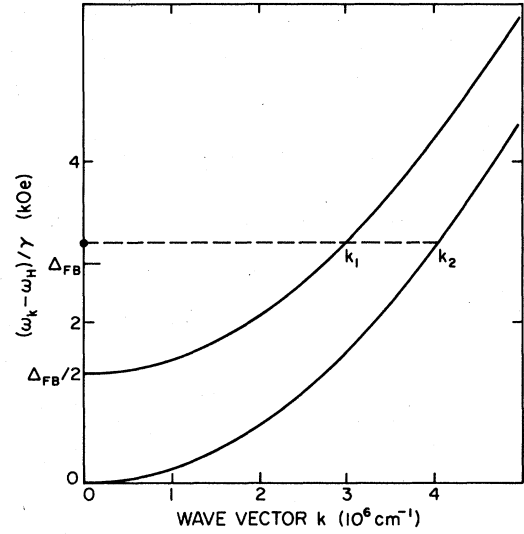where V describes the perturbative effects of the impurity,

FIG. 5. Calculated degenerate manifold of spin-wave states in the long-wavelength region for FeF_2. Note that the scale of k is 10^3 larger than in Fig. 1. k_1 and k_2 represent the limits of the continuum of states into which a $k \simeq 0$ mode can decay via two-magnon scattering. $\Delta_{FB} = 4\pi MH_A/H_C$.

and can be expressed in terms of magnon operators $\alpha_{\vec{k}}$ and $\alpha_{\vec{k}}^\dagger$ (for the down-going branch) as

$$V = \sum_{\vec{k}, \vec{k}'} F_{\vec{k} \vec{k}'} (\alpha_{\vec{k}'} \alpha_{\vec{k}}^\dagger + \alpha_{\vec{k}} \alpha_{\vec{k}'}^\dagger), \quad (5)$$

where $F_{\vec{k} \vec{k}'}$ is the Fourier transform of the scattering potential. The rate at which the mode k_0 decays into a degenerate mode k through two-magnon scattering (5), given by the standard golden rule, can be expressed as a linewidth

$$\Delta H(\omega) = \frac{\Omega}{\gamma \hbar^2 (2\pi)^2} \int |F_{\vec{k}_0 \vec{k}}|^2 \delta(\omega - \omega_k) d^3k, \quad (6)$$

where Ω is the volume of the sample and ω is the frequency of the mode k_0. Since we are interested in the decay of modes in the polariton region, we have $k_0 (\simeq 10^3$ cm$^{-1}) \ll k (\simeq 10^6$ cm$^{-1})$, as can be seen from the plots in Figs. 1 and 5. Furthermore, for point imperfections the strength of the scattering potential is approximately k independent for $ka \ll 1$, and we may set $F_{\vec{k}_0 \vec{k}} \simeq F_0$ in Eq. (6). If we use the dispersion relation (3), with the approximation $H_c^2 \gg 4\pi MH_A$, $2H_E^2 b^2 k^2$, the density of degenerate states becomes

$$\rho(\omega) = \int d\phi_k d(\cos\theta_k) \delta(\omega - \omega_k)$$

$$= \frac{H_c}{\gamma MH_A} \left[\frac{2\pi MH_A}{2\pi MH_A + H_E^2 b^2 k^2 - (\omega - \omega_H)H_c/\gamma} \right]^{1/2}. \quad (7)$$

As discussed in Refs. 16 and 17, Eq. (7) differs from the expression used by Loudon and Pincus,[11] who neglected the anisotropic nature of the spectrum and made the approximation that all degenerate states lie at the maximum value of k. Though this is a reasonable approximation, we have chosen to keep the full expression (3) in carrying out our numerical calculations. The integral in (6) is evaluated over the range $|\vec{k}| = k_1$ to $|\vec{k}| = k_2$, where

$$k_1 = (H_c \omega_0/\gamma - 2\pi M H_A)^{1/2}/H_E b ,$$

$$k_2 = (H_c \omega_0/\gamma)^{1/2}/H_E b , \qquad (8)$$

and $\omega_0 = \omega - \omega_H$ is the energy of the mode that relaxes, relative to the bottom of the spin-wave manifold. Using (7) and (8) in (6), one may obtain the following contribution of a single impurity scatterer to the linewidth:[17]

$$\Delta H_0 = \frac{\Omega H_c |F_0|^2}{4\pi(\gamma\hbar)^2(2\pi M H_A)^{1/2}H_E^3 b^3} \left[(2\pi M H_A H_c \omega_0/\gamma)^{1/2} + (H_c\omega_0/\gamma - 2\pi M H_A)\left[\frac{(H_c\omega_0/\gamma)^{1/2} + (2\pi M H_A)^{1/2}}{(H_c\omega_0/\gamma - 2\pi M H_A)^{1/2}} \right] \right] . \qquad (9)$$

For a sufficiently small impurity concentration c the contributions to the linewidth are approximately additive, so that

$$\Delta H(\omega) = cN \Delta H_0 . \qquad (10)$$

Clearly this linewidth increases as ω increases. The scattering potential $F(\vec{k}) \simeq F_0$ can be found from V in the representation given by Eq. (5). For an impurity with exchange interaction J' to a number z of equivalent neighbors,

$$F_0 \sim (J - J')Sz/N , \qquad (11)$$

where J is the exchange parameter between host neighbors. With (9)–(11) and the parameters appropriate[18] to FeF_2:Mn we find that ΔH is of the order of a few Oe for polariton energies near the top of the forbidden band. This is *three orders of magnitude smaller* than the fit to the observed polariton line shape requires—a discrepancy which is remedied by taking proper account of multiple scattering.

The very existence of a localized mode signals the breakdown of perturbation theory, a bound-state singularity in the scattering matrix associated with the impurity potential. On the one hand, we should not be surprised with the inadequacy of a perturbation calculation at energies near that of the local magnon; on the other hand we know that to treat the strong but spatially local perturbation adequately we need only introduce the t matrix, which incorporates multiple-scattering effects to all orders. Thus the continuum wave functions $|\psi_k\rangle$ in the presence of the impurity potential are given by the Lippmann-Schwinger equation,[19]

$$|\psi_{\vec{k}}\rangle = |\vec{k}\rangle + (E - \mathcal{H}_0 + i\eta)^{-1} V |\psi_{\vec{k}}\rangle , \qquad (12)$$

with the Hamiltonian breakup of Eq. (4) and $\eta = 0^+$. We introduce the t matrix as the operator which acts on the unperturbed states $|\vec{k}\rangle$ to give the same result as V acting on the distorted state $|\psi_{\vec{k}}\rangle$,

$$T|\vec{k}\rangle = V|\psi_{\vec{k}}\rangle \qquad (13)$$

so that T accounts for multiple impurity scattering to all orders. From Eqs. (12) we have

$$T = (1 - VG^0)^{-1}V , \qquad (14)$$

where $G^0 = (E - \mathcal{H}_0 + i\eta)^{-1}$ is the pure-crystal Green function. Then multiple-scattering results are included by replacing V by T in the first-order time-dependent perturbation expression for the transition probability; i.e., the squared matrix element becomes

$$|\langle \vec{k}|T|\vec{k}_0\rangle|^2 = |\langle \Psi_{\vec{k}}|V|\vec{k}_0\rangle|^2 . \qquad (15)$$

Of course, far from a scattering resonance or a bound state $T \simeq V$, and the modification to ordinary first-order perturbation theory is small. However, here the effect is enormous, as the existence of a local mode implies, and as a consequence, the linewidth is enhanced by three orders of magnitude.

The calculation of T from Eq. (14) is lengthy but straightforward. The system is well described by a Hamiltonian[10,18] which includes isotropic exchange, single-ion uniaxial anisotropy along the c axis of the lattice (chosen here as the z direction), and the Zeeman interaction with a magnetic field H_0 applied also along the c axis,

$$\mathcal{H} = \mu_B H_0 \sum_l g_l S_l^z + 2J_2 \sum_{l,\delta} \vec{S}_l \cdot \vec{S}_{l+\delta} - D \sum_l (S_l^z)^2$$
$$+ 2J_2' \vec{S}_0 \cdot \sum_{\delta_2} \vec{S}_{\delta_2} + 2J_1' \vec{S}_0 \cdot \sum_{\delta_1} \vec{S}_{\delta_1} - D'(S_0^z)^2 , \qquad (16)$$

where sites are labeled by subscripts of the spin operators and a single impurity is located at the origin ($l = 0$). We have retained only the dominant exchange terms, between next-nearest neighbors on opposite sublattices of the body-centered tetragonal arrangement of magnetic atoms, for the pure FeF_2 host, or between Fe spins. The impurity spin is taken to couple with its eight next-nearest neighbors at positions δ_2, and its two nearest neighbors at positions δ_1. In a lattice site representation the perturbation V due to a single Mn impurity in FeF_2 is a matrix of rank 11, involving the impurity and its δ_1 and δ_2 neighbors. Explicitly, to quadratic order in the boson operators of the Holstein-Primakoff representation we have for a single impurity on the "up" sublattice

$$V = [16S(J_2' - J_2) + 4SJ_1' + 2(D'S' - DS) + (g' - g)\mu_B H_0]a_0^\dagger a_0 + 2J_1(SS')^{1/2} \sum_{\delta_1}(a_0^\dagger a_{\delta_1} + a_{\delta_1}^\dagger a_0)$$

$$+ 2[J_2'(S'S)^{1/2} - J_2 S] \sum_{\delta_2}(a_0^\dagger b_{\delta_2}^\dagger + b_{\delta_2} a_0) + 2(J_2' - J_2) \sum_{\delta_2} b_{\delta_2}^\dagger b_{\delta_2} - 2J_1' S' \sum_{\delta_1} a_{\delta_1}^\dagger a_{\delta_1} . \tag{17}$$

The matrix $\underline{V}$ formed in the usual way by the coefficients of the boson operators in Eq. (17) can be block diagonalized[20] by the unitary matrix $\underline{U}$ formed from the basis vectors of the point-symmetry group of the impurity cluster:

$$\underline{V}' = \underline{U}\,\underline{V}\,\underline{U}^{-1} . \tag{18}$$

Then this same transformation, also by block diagonalization, simplifies the inversion of the matrix $(\underline{1} - \underline{V}\,\underline{G}^0)$ which determines T through Eq. (14). The lattice-site representation for T is recovered by inverting the unitary transformation

$$\underline{T} = \underline{U}^{-1}\underline{T}'\underline{U} . \tag{19}$$

Because we are dealing with a two sublattice antiferromagnet, in the pure system there are two excitations associated with each wave vector $\vec{k}$. Since the matrix elements $T_{\vec{k}\,\vec{k}'}$ corresponding to the $F_{\vec{k}\,\vec{k}'}$ of Eq. (5) are the scattering matrix elements for only one of the two excitation branches, they are not simply the Fourier transforms of T_{ij}. Rather, these must be appropriately weighted by the magnon transformation coefficients $u_{\vec{k}}$ and $v_{\vec{k}}$. Since the magnons involved in the scattering process are near the center of the Brillouin zone we can simplify the result with $k \simeq k' \simeq 0$. The contribution of the local mode enhanced two-magnon scattering to the linewidth is then given by Eq. (9) with
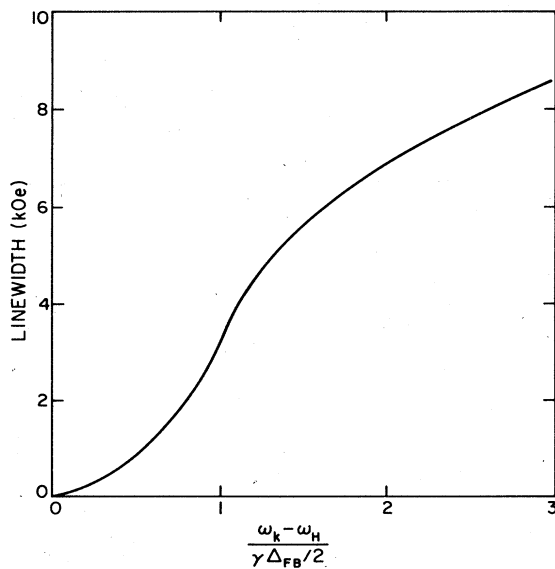
$$F_0 = \frac{1}{N}\left[u_0^2 \sum_{i,i'} T_{ii'} - u_0 v_0 \sum_{i,j}(T_{ij} - T_{ji}) - v_0^2 \sum_{j,j'} T_{jj'}\right] , \tag{20}$$

where i,i' and j,j' refer to the up and "down" spin sublattices, respectively. We have applied the results above to FeF_2:Mn and compared with the experimentally observed magnon linewidths using the following parameters:[18] $S=2$, $J_2=1.82$ cm^{-1}, $J_1=0$, $g=2.25$, $D=6.5$ cm^{-1}, $S'=2.5$, $J_2'=1.79$ cm^{-1}, $J_1'=0.2$ cm^{-1}, $g'=2.0$, and $D'=0.19$ cm^{-1}. Figure 6 shows the calculated linewidth for $c=0.5$ at. % as a function of the mode frequency relative to the bottom of the magnon band, in units of $\gamma \Delta_{FB}/2$ (the width of the spin-wave manifold). We note that the contributions from exchange, anisotropy, and g-factor scattering are equally important for the linewidth, which now has the magnitude of a few kOe and is strongly frequency dependent. In Fig. 7 we compare the experimentally measured transmission line shape obtained for the sample with $c=0.5$ at. % to the theoretical prediction of the polariton model with a frequency-dependent relaxation parameter given by the above theory. As can be seen, the agreement between theory and experiment is remarkably good.

In summary, we have shown that the main relaxation mechanism of $k \simeq 0$ magnons in FeF_2:Mn at low temperatures is impurity-induced two-magnon scattering. Because of the proximity of the impurity-associated local mode to the magnon band, the scattering is greatly enhanced and the usual first-order perturbation[11] calcula-
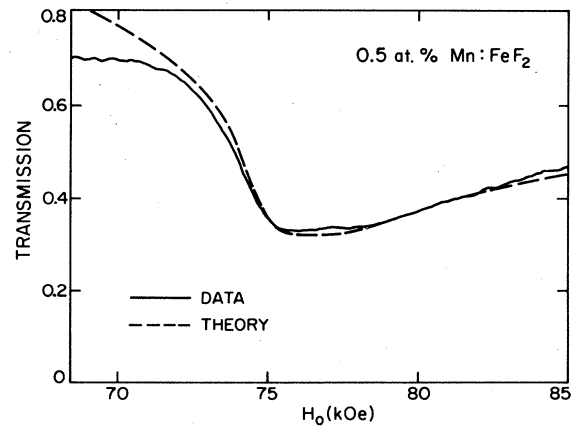

FIG. 6. Linewidth due to two-magnon impurity multiple scattering in 0.5 at. % Mn:FeF$_2$ as a function of position of the magnetic mode relative to the bottom of the spin-wave band.

FIG. 7. Comparison of transmission data from a 80-μm-thick sample of 0.5 at. % Mn:FeF$_2$ (solid curve) with the theoretical prediction of polariton model with a frequency-dependent relaxation parameter obtained from the two-magnon impurity multiple-scattering calculation.

tion of the magnon linewidth fails. However, multiple-scattering effects can be calculated with a t-matrix theory and the resulting relaxation rate has the magnitude and the strong frequency dependence required to explain the experimentally observed line shapes. It is noteworthy that the polaritons play no role in the actual mechanism. They enter in the calculation of the line shape only because in a FIR transmission experiment the radiation excites mixed magnetic-electromagnetic modes in the sample. The large, frequency-dependent damping is produced by im-purity scattering of the magnetic modes, and should be observed in experiments which probe magnons far from the polariton region. In fact this has been recently confirmed in high-resolution light scattering experiments.[21]

[1]R. C. Ohlmann and M. Tinkham, Phys. Rev. **123**, 425 (1961).

[2]B. Enders, P. L. Richards, W. E. Tennant, and E. Catalano, in *Magnetism and Magnetic Materials—1972 (Denver)*, Proceedings of the 18th Annual Conference in Magnetism and Magnetic Materials, edited by C. D. Graham and J. J. Rhyne (AIP, New York, 1972), p. 179.

[3]R. W. Sanders, V. Jaccarino, and S. M. Rezende, Solid State Commun. **28**, 907 (1978).

[4]R. W. Sanders, R. M. Belanger, M. Motokawa, V. Jaccarino, and S. M. Rezende, Phys. Rev. B **23**, 1190 (1981).

[5]D. L. Mills and E. Burstein, Rep. Prog. Phys. **37**, 817 (1974).

[6]R. M. Toussaint and V. Jaccarino, J. Appl. Phys. **55**, 2458 (1984).

[7]R. M. Belanger, V. Jaccarino, and S. Geschwind, J. Magn. Magn. Mater. **31−34**, 681 (1983).

[8]C. Wiecko and D. Hone, J. Phys. C **13**, 3883 (1980).

[9]P. Thayamballi and D. Hone, Phys. Rev. B **27**, 2924 (1983).

[10]S. M. Rezende, D. Hone, and R. M. Toussaint, Phys. Rev. B **29**, 1638 (1984).

[11]R. Loudon and P. Pincus, Phys. Rev. **132**, 673 (1963).

[12]R. W. Sanders, D. Paquette, V. Jaccarino and S. M. Rezende, Phys. Rev. B **10**, 132 (1974).

[13]M. Sparks, *Ferromagnetic Relaxation Theory* (McGraw Hill, New York, 1964).

[14]J. P. Kotthaus and V. Jaccarino, Phys. Rev. Lett. **28**, 1649 (1972).

[15]J. P. Kotthaus, Ph.D. thesis, University of California, Santa Barbara, 1972 (unpublished).

[16]R. W. Sanders, Ph.D. thesis, University of California, Santa barbara, 1978 (unpublished).

[17]R. M. Toussaint, Ph.D. thesis, University of California, Santa Barbara, 1982 (unpublished).

[18]S. M. Rezende, Phys. Rev. B **27**, 3032 (1983).

[19]See, for example, J. Callaway, *Quantum Theory of the Solid State* (Academic, New York, 1976).

[20]E. Shiles and D. Hone, J. Phys. Soc. Jpn. **28**, 51 (1970).

[21]S. M. Rezende and E. F. da Silva, Jr. (unpublished).